3-5 Development of Instrument for the Resonance Scattering Emission of Oxygen Ion (O Ⅱ:83.4nm) — Toward the Imagery of Magnetosphere —

YAMAZAKI Atsushi, MIYAKE Wataru, YOSHIKAWA Ichiro, NAKAMURA Masato, and TAKIZAWA Yoshiyuki

According to previous theories a large number of oxygen ions are not able to escape from the ionosphere to the magnetosphere due to its heavy mass and loss process in the upper atmosphere. Recent satellite observations, however, reveal that oxygen ions of the ionospheric origin exist in the magnetosphere, and that the outflow flux from the polar ionosphere is comparable to that of hydrogen ions, which have its light mass, during the high solar activity and the high geomagnetic activity. The distribution of oxygen ions provides the interpretation of the plasma transfer during the high activity, and gives us the effective information for monitoring the space weather. The remote-sensing method is useful for the measurement of the distribution of oxygen ions all over the magnetosphere. We advance development of new optics for the resonance scattering emission of oxygen ions.

Keywords
Oxygen ion, Resonance scattering, Extreme ultraviolet, Remote sensing, Imaging

1 Introduction

The behavior of the plasma that surrounds the Earth from an altitude of several tens of kilometers in the ionosphere to the magnetosphere is a major topic of interest for scientists studying Solar Terrestrial plasma physics. Particularly important is the response of plasma in the Earth's magnetosphere to solar wind plasma and resulting phenomena such as magnetic field line reconnection, generation of the field-aligned current (FAC) system, acceleration of charged particles above the polar regions, and accompanying auroral illumination. Over the past 30 years, plasma observations seeking to clarify the mechanisms of these phenomena have primarily been made by direct, or *in-situ*, measurement of plasma by satellites deployed in the region where these phenomena occur. However, since these observations have only been able to provide instantaneous data for single observation points, they have been inadequate for separating the components of temporal variations from spatial variations of magnetospheric response to the solar wind changes.

Alongside these *in-situ* observations, various efforts have sought to understand the global plasma distribution near Earth space by visualization. One major success in these efforts revealed the good correlation between the temporal evolutions of auroral illumination and magnetospheric activity. This discovery was based on observation by a polar-orbiting satellite passing above the polar region[1][2]. Such remote-sensing observations have been made at visible to ultraviolet wavelengths, but not in the extreme ultraviolet (EUV) region. The resonance-scattering emission lines vital to plasma observation—the 30.4-nm (He Ⅱ) and 58.4-nm (He Ⅰ) Lyman α lines of helium ions and atoms and the 83.4-nm (O Ⅱ) line of

oxygen ions—are found in the EUV region. These emission lines correspond to energy gaps with the highest transition probability for particles in the ground state. The concept of visualizing the tenuous plasma environment was originally conceived with the detection of these scattered emissions[3]. The technical difficulties of developing optical equipment have restricted such efforts involving EUV observations at the initial stages. However, developments in nanotechnology over the past 10 years have enabled the production of a multilayer-coated mirror that can efficiently collect EUV light, leading to discussions of the possibility of or need for studying the behavior of plasma by imaging the global plasma environment near Earth in EUV[4][5][6].

In resonance-scattering emission observations, care must be taken to account for changes in an emission rate factor due to Doppler shifts. The major light source for resonance-scattering emission lines is solar radiation. Doppler shifts must be taken into consideration in a system that moves with plasma relative to the Sun. If the speed of the plasma, the scattering material, is such that the resulting Doppler shift exceeds the solar spectral width, the plasma cannot induce resonance scattering. This is apparent in the range of solar radiation spectrum that consists of isolated emission lines, like that for He Ⅱ. However, the spectrum in the O Ⅱ region consists of several lines that appear as a single line, due to degeneracy of multiple resonance states. Also present is a continuous spectrum of hydrogen atom. Even when a Doppler shift occurs, a different emission line or a continuous band will overlap with the wavelength for resonance scattering, maintaining the resonance-scattering emission rate factor at a certain level. Thus, unlike helium ions, oxygen ions can be used as tracers for imaging plasma outflow from the polar ionosphere and the plasma distribution and transport in the magnetotail[5][7].

Resonance scattering of helium ions (He Ⅱ) is a strong candidate for imaging the plasmasphere that surrounds the Earth, since helium ions comprise nearly a tenth of all ions in the plasmasphere, and since their low kinetic energy provides immunity from negative Doppler shift effects. The XUV (eXtreme Ultraviolet Scanner) onboard the Planet-B satellite[8][9][10] and the EUV (Extreme Ultraviolet Imager) on the IMAGE (Imager for Magnetosphere and Aurora) satellite[11][12][13] have made successful imaging observations based on He Ⅱ, providing information on real-time 2-D behavior in the plasmasphere.

On the other hand, the resonance scattering of oxygen ions (O Ⅱ: 83.4 nm) is better suited for visualizing plasma with high kinetic energy, such as plasma escape from the ionosphere or present within the magnetosphere. More significantly, contrary to theoretical predictions, oxygen ions play a more important role in the magnetosphere than hydrogen or helium ions. The escape of plasma from the polar ionosphere is known as the polar wind. Theoretical studies during the 1960s had predicted that plasma consisting of low-mass particles such as protons and helium ions would prove to be the main constituent of the polar wind, and that the amount of escape flux of heavier oxygen ions was only several percent of the proton and helium ion flux[14][15]. However, observations by polar-orbiting satellites (Akebono, Dynamic Explorer-1 and 2) show large amounts of oxygen ions escaping from the polar ionosphere[16][17][18]. This phenomenon can be explained only if acceleration and heating of oxygen ions occur at altitudes below 1,000 km[19]. The precise mechanism has yet to be clarified. The Geotail satellite detected the presence of large amounts of cold oxygen ions in the magnetotail, especially in the lobe/mantle region, which were observed to flow towards the magnetotail with the beam-like distribution[20][21][22]. Based on comparisons with α particles of solar wind origin penetrating into the magnetosphere, these oxygen ions have been identified as originating from the Earth's ionosphere. However, an as-yet unidentified mechanism of acceleration and heating must account for their existence[23][24]. Further-

more, the comparison of the density of the oxygen ions in the magnetosphere with the balance between the escape to interplanetary space and the supply from the ionosphere based on *in-situ* measurement data have shown that the number of oxygen ions entering the magnetosphere is an order of a magnitude greater than that exiting it, indicating an unidentified reservoir or transport route for oxygen ions[25]. The discovery of cold helium ions within the plasma sheet by the Planet-B satellite[26] also supports the hypothesis of an unknown reservoir of plasma. These studies indicate that cold plasma, the presence of which were not previously confirmed by *in-situ* observation due to the satellite's potential, exists within the magnetosphere, and imply that the behavior of oxygen ions within the magnetosphere may serve as an effective tracer for resolving the mechanism of plasma acceleration and heating.

It must be noted that since imaging observations can only provide information on column density in the line-of-sight direction, they complement *in situ* measurements in the magnetosphere (Fig.1). If the position and timing of satellites in the magnetosphere making *in-situ* observations of the magnetotail dynamics can be determined by imaging, data obtained by direct plasma observations could be interpreted more effectively. Conversely, providing information on plasma density and velocity at each observation point of the satellites in the magnetosphere as the boundary conditions for imaging will make it possible to create 3-D images from the 2-D images obtained.

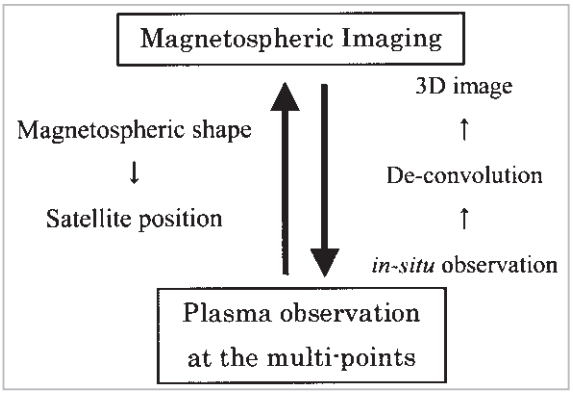

Fig.1 *Relationship between imaging observation and in-situ particle observation*

2 Resonance Scattering of Oxygen Ions

2.1 Oxygen Ion Emission Lines in Solar Radiation

The Sun is the major light source inducing resonance scattering of oxygen ions in space near the Earth. The solar radiation spectrum exhibits emission lines for monovalent and divalent oxygen ions (O Ⅱ and O Ⅲ) near the 83.4-nm wavelength. Since the energy levels of each ion are degraded, multiple emission lines exist in close proximity. A model of the detailed spectrum of this bandwidth has been proposed based on the results of rocket observations in the 1960s[7][27]. The continuous Lyman spectrum component of hydrogen is also known to exist in this wavelength region [28]. Fig.2 shows an example of a spectrum during a solar minimum—a sum of the emission line spectrum model and values observed for the continuous spectrum. Seven emission lines are visible between 83.26 nm and 83.55 nm. (There are in fact 9 emission lines, but 2 are within the emission line width and cannot be resolved.)

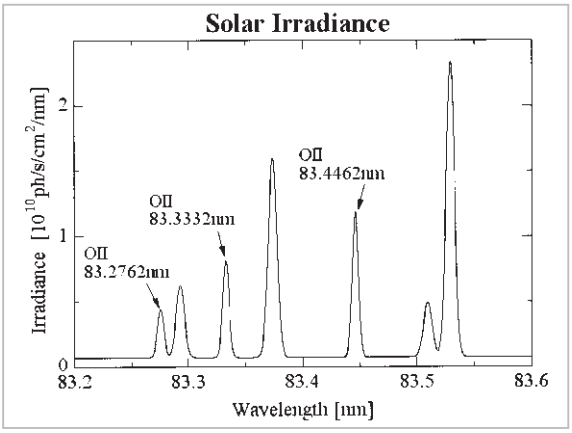

Fig.2 *The solar radiation spectrum near 83.4 nm*

Of the 7 emission lines, the 3 lines at 83.2762, 83.3332, and 83.4462nm correspond to those of O Ⅱ, and the others to O Ⅲ. If a monovalent oxygen ion were motionless relative to the Sun, resonance scattering would

only occur with the above 3 emission lines. However, if the ion is in motion relative to the Sun, the above emission lines would be affected by Doppler shift in a system moving with the oxygen ion. As the original wavelength is λ_0, the wavelength λ after the shift can be expressed as:

$$\lambda = \lambda_0 \left(1 - \frac{v}{c}\right) \qquad (2.1)$$

Here, v is the velocity of the oxygen ion relative to the Sun with a positive value towards the Sun, and c is the speed of light. If, for example, the oxygen ions were moving away from the Sun at 300 km/s, the O Ⅲ emission line near 83.37 nm would shift to a wavelength 0.0834 nm longer in the system, overlapping with the resonance-scattering emission line at 83.4462 nm. In other words, the emission rate factor of resonance scattering, or the g-factor, depends on the velocity relative to the Sun, the radiation source. Additionally, since the oxygen ions in the magnetosphere and the ionosphere have a finite temperature, the effect of Doppler broadening will be present. Even if the central wavelength does not match precisely, scattering will occur in photons with wavelengths within the Doppler width, and emission rate factor will also display temperature dependency. Thus, calculations of the g-factor must take into account the effects of both the Doppler shift and Doppler width. The g-factor is represented by the following equation:

$$g = \int \sum_i \sigma_{0i} \exp\left[-\left(\frac{\lambda/\lambda_{0i} - 1}{v_{th}/c}\right)^2\right] F_\lambda[\lambda(1 + v/c)]d\lambda \qquad (2.2)$$

Here, i represents the number of O Ⅱ emission lines, v_{th} the thermal velocity, and F_λ the solar radiation photon flux per unit wavelength. Representing the scattering cross section at the central wavelength for each emission line, σ_{0i} can be expressed as:

$$\sigma_{0i} = \frac{\pi e^2}{m_e c} \cdot \frac{f_i}{\sqrt{\pi}\frac{v_{th}}{c}\lambda_{0i}}, \qquad (2.3)$$

where m_e, e, and f_i, respectively, represent the mass of the electron, the elementary electric charge, and the harmonic oscillator strength of the i th emission line.

Fig.3 shows the g-factor as a function of velocity relative to the Sun at oxygen ion temperatures of 1, 100, and 1000 eV. The velocity vector is positive towards the sun (i.e., the heading is towards the Sun). The dependence of the g-factor on the temperature of the scattering particles is influenced by the relationship between the widths of the solar radiation spectra. The g-factor shows a complex variation pattern at low temperatures, while changing smoothly at higher temperatures. Note that the g-factor is higher when the velocity is 300 km/s, compared to stationary conditions, since resonance scattering occurs with the O Ⅲ emission line of the solar radiation with high illumination intensity.

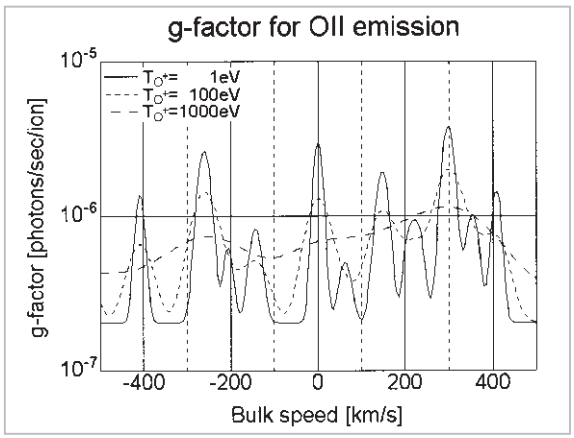

Fig.3 *Emission rate factor (g-factor) with Doppler shift effects*

Given the g-factor calculated above, the intensity of the scattered light is given by:

$$4\pi I = \int_{\text{line of sight}} ngdz \qquad (2.4)$$

Here, n is the oxygen ion density and g the g-factor. Both are functions of line-of-sight distance z from the observer. The integration is performed from the position of the observation instrument to an infinite point.

2.2 Development of the Observation Instrument

The difficulty of developing an imaging instrument for measuring the resonance-scattering emission of oxygen ions arises from the necessity of accounting for the effects of the geocorona emitted by hydrogen gases surrounding the Earth. The geocorona consists of the hydrogen Lyman α line (Ly-α ; wavelength of 121.57 nm) close to the 83.4-nm O Ⅱ emission line. Furthermore, its maximum intensity has been reported to be 10 kRayleighs (kR)[29]. As will be explained later, the O Ⅱ emission for observation is extremely weak. Thus, the required ratio of sensitivity to O Ⅱ and Ly-α is extremely large, 10^5-10^6. Development is further hindered by the need for optics that use a collector mirror and for an optical element with a bandpass in the O Ⅱ emissions due to weak emissions. But no material exists that is transparent to or has high reflective efficiency for 83.4-nm light. A primary-focus reflective optical system, consisting of a main mirror, a bandpass filter, and a detector, is adopted to overcome this problem. The optical elements that determine the sensitivity of the instrument are the coating of the main mirror and the filter material.

Based on a consideration of optical properties[30][31], molybdenum was selected as the most appropriate coating material for the main mirror. An indium thin film was selected for the bandpass filter. Both materials are relatively unaffected by aging and have high reflectivity and transmissivity to the O Ⅱ emission region. We have built an instrument that has to date achieved a sensitivity ratio of O Ⅱ to Ly-α of 10^6. The optical system has a mirror reflector with a 100-nm thick molybdenum coating at its center, a 275-nm thick indium filter, and a channel electron multiplier (CEM) as a detector. Fig.4 is a cross-section of the optical system. Figs.5 and 6 present the results of measurements of mirror reflectivity and filter transmissivity. The wavelength dependence of reflectivity and transmissivity is determined by the optical constant specific to the metals. The general sensitivity characteristic of the instrument is shown in Fig.7. This instrument, onboard a SS-520-2 sounding rocket which was launched from the northern polar region and with an apex at an altitude of 1,000 km, successfully detected resonance-scattering emission of oxygen ions from the upper ionosphere. Marking the first step in imaging observation of oxygen ions escaping from the ionosphere, the observation results indicate that oxygen ions are distributed above the polar ionosphere[32].

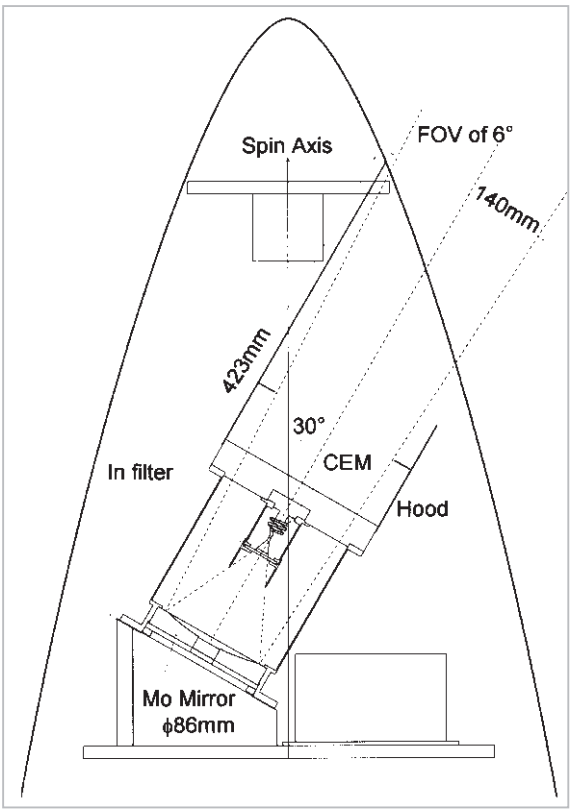

Fig.4 *Cross-section of the observation instrument on the SS-520-2 rocket*

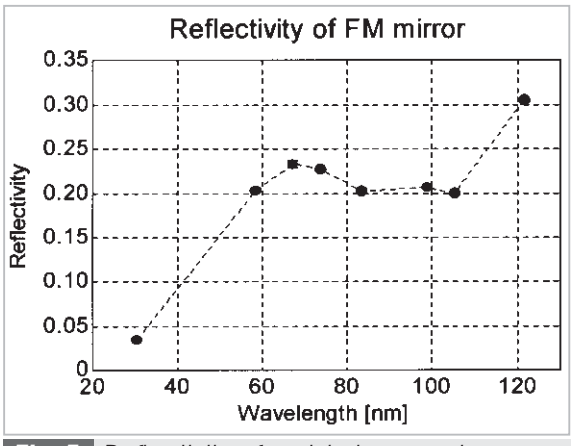

Fig.5 *Reflectivity of molybdenum mirror*

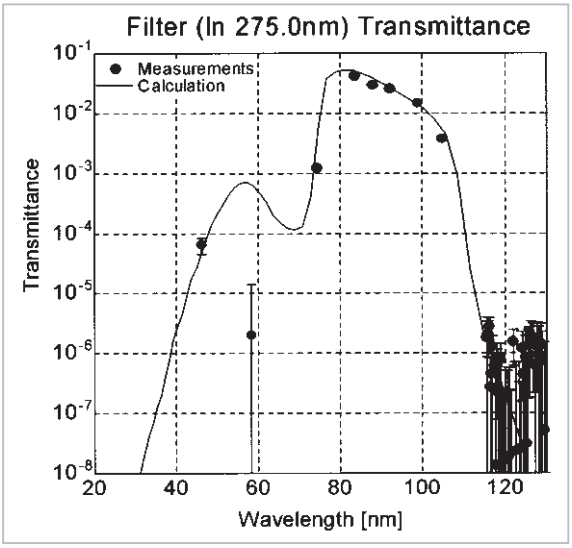

Fig.6 *Transmissivity of indium filter*

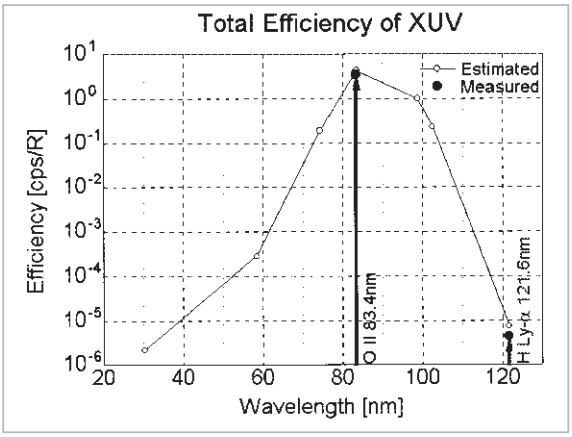

Fig.7 *Sensitivity of the observation instrument on the SS-520-2 rocket*

Studies have also sought to improve sensitivity to O Ⅱ. As shown in Fig.8, a Ni/MgF_2 coating on an aluminum substrate provides reflectivity at H Ly-α two orders of magnitude lower than that of the earlier mirror[33]. If this mirror can be successfully applied to practical applications, the removal of the H Ly-α line presently performed by the indium filter may also be performed simultaneously at the mirror, making it possible to reduce the removal rate at the filter. In other words, it will be possible to reduce the thickness of the indium filter while retaining the sensitivity ratio of O Ⅱ to H Ly-α at the onboard instrument level, thereby improving absolute sensitivity to O Ⅱ. Table 1 shows the expected sensitivity to O Ⅱ in this case, comparing it to that of the instrument aboard the SS-520-2 rocket. The mirror reflectivity and quantum efficiency of the detector are equal, but the thinner filter increases transmissivity, with sensitivity expected to increase by a factor of around 5. The problem of interfacial diffusion in the coating over time has been reported as a potential problem for practical applications [34]. This problem represents another topic for future group investigation.

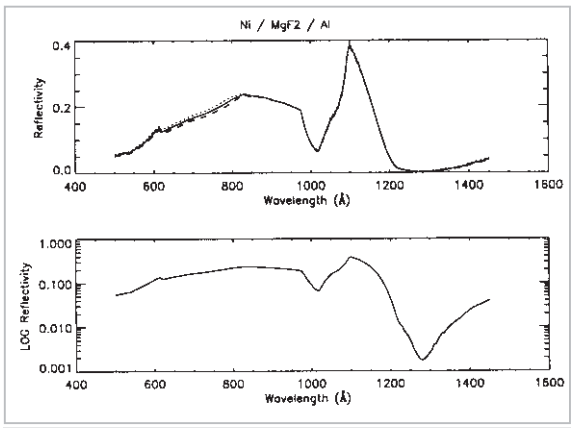

Fig.8 *The reflective characteristics of mirror with a Ni 70Å/MgF_2 105Å coating on an aluminum substrate*

Table 1 *Sensitivity comparison of the mirror aboard the SS-520-2 rocket and the new mirror*

O II emission	SS-520-2	New Mirror
Reflectivity	0.2	0.2
Transmittance	0.05	0.2
Detector Efficiency	0.04	0.05
Total Efficiency	0.0004	0.002

3 Polar Wind Imaging

3.1 Escape from the Polar Ionosphere

In the 1960s, the escape flux of oxygen ion was predicted to be only several percent of that of protons and helium ions[14]. This prediction was based on the large mass of the oxygen ion and the ease with which oxygen ions become neutral through charge exchange [15]. However, observations by polar-orbiting satellites in the 1980s indicated that these predictions were not always correct. The observation results by Dynamic Explorer-1 and 2 revealed that during high solar activity, or

when the magnetosphere has been actively disturbed, the oxygen ion flux increases[16]. The velocity of oxygen ions parallel to magnetic field lines calculated from observation data of the Akebono satellite showed that oxygen ions were accelerated below an altitude of 4,000 km[18]. Rocket observations revealed the presence of an acceleration regime near an altitude of 1,000 km. The acceleration mechanism of oxygen ions was found to be the key to determining plasma flux from the ionosphere[19]. Fig.9 shows the distribution of the oxygen ion escape flux determined from statistical analysis of Akebono observation data [17]. Escape flux is high near the dayside cusp region and the duskside, reaching 10^8 /cm^2/s, and is low at midnight or in high-latitude regions.

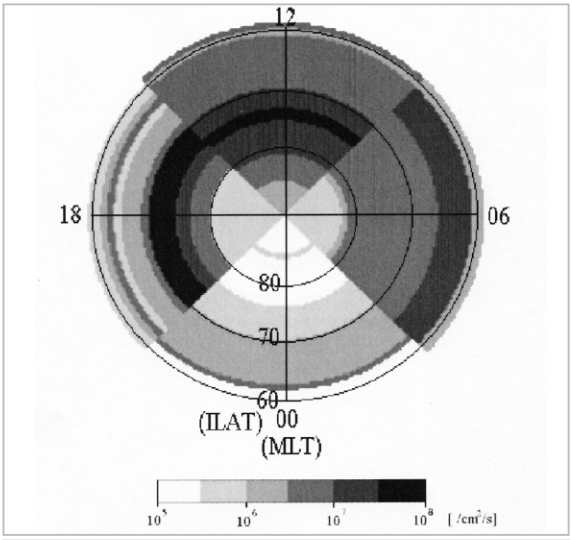

Fig.9 *Distribution of oxygen ion escape flux from the polar ionosphere based on Akebono satellite observation data*

3.2 Intensity of Scattered Light of Escaping Oxygen Ions

A model will be devised for the density distribution and g-factor required for Eq. (2.4) to calculate O-Ⅱ scattering intensity. The density distribution was determined based on the pressure gradient, polarization electric field, and gravity, using the results of statistical analysis of Akebono observation data shown in Fig.9 as boundary conditions. The plasma condition is assumed to be quasi-neutral. The escaping oxygen ions from the ionosphere are assumed to have temperatures of 4,000 K and energy of 10 eV. Escape velocity and temperature at an arbitrary position can be determined simultaneously, and the g-factor can be estimated from Eq. (2.2). Fig.10 shows the intensity distribution of scattered emissions calculated based on these assumptions. The half-circle in the middle of the lower part of each plot represents Earth, while the white lines stretching from the half-circle show the magnetic field lines of the Earth, assuming a dipole. The plot ranges are ±5 R_E (Earth radii) in the equatorial plane and 5 Re in the direction of the pole. The top and bottom panels show the intensity of scattered emissions of oxygen ions for observation when the line-of-sight is in the day-night and morning-dusk directions, respectively. This result indicates that the maximum intensity is 1 R. Thus, it has been concluded that in order to make observations of regions several R_E away from the Earth in order to identify the escape route of oxygen ions, instruments must be able to measure intensities around 0.1 R. Each mag-

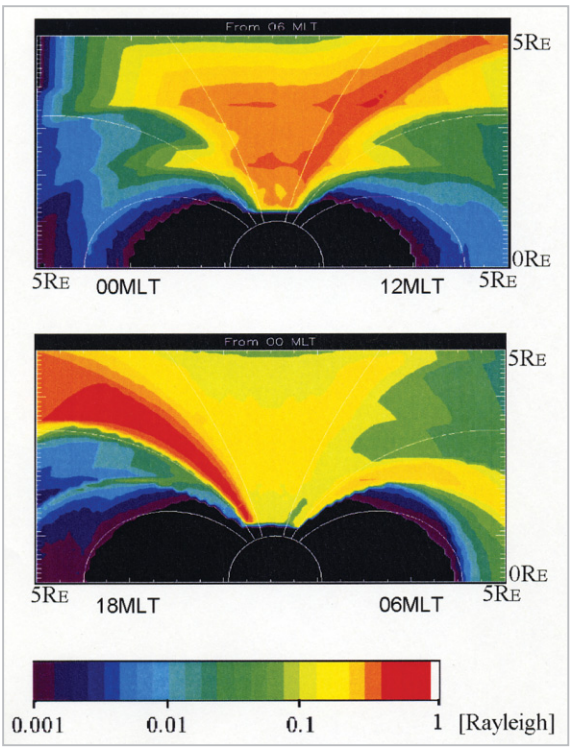

Fig.10 *The predicted intensity distribution of scattered light*

netic force tube was found to display a different illumination pattern. This may help to identify the spatial structure of the oxygen ion escape mechanism.

4 Magnetosphere Imaging

4.1 Oxygen Ions Distributed in the Magnetotail

Oxygen ions with large mass are not able to attain sufficient velocity to escape Earth's gravity only by accelerating from the pressure gradient along open magnetic field lines extending from the Earth to interplanetary space. Previously, it had been believed that they would be unable to escape from Earth and would instead enter the plasma sheet by ExB drift[35][36]. However, the Geotail satellite observation has revealed the presence of oxygen ions of ionospheric origin in the lobe/mantle region of the magnetotail[22] [23]. Figs.11, 12, and 13 show the temperature, density, and velocity of the observed oxygen ions[37]. The horizontal axes of all three plots are distant from the Earth and show the results of observation in the range of 0-220 R_E. Fig.11 shows that the oxygen ion temperature is low. While the data is mostly plotted within the 10-100 eV range, results of linear fitting shown by a line in the plot indicate that the temperature displays a rising trend away from the Earth. Fig.12 shows that oxygen ion density decreases with increasing distance from Earth. The average densities at 50 R_E and 200 R_E are 3×10^{-3}/cm^3 and 3×10^{-4} /cm^3, respectively. It can be seen from Fig.13 that the average velocity from the Earth towards the tail changes significantly, from 120 km/s near Earth at 20 R_E to 280 km/s deep in the magnetotail at 200 R_E. However, deviations are

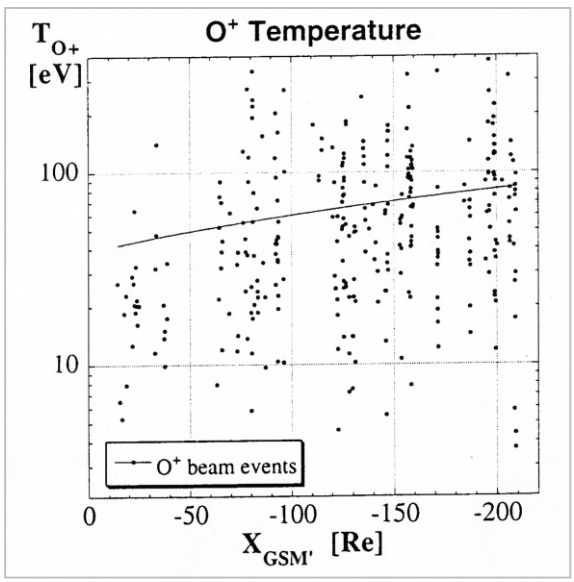

Fig.11 *Temperature distribution of oxygen ions in the magnetotail*

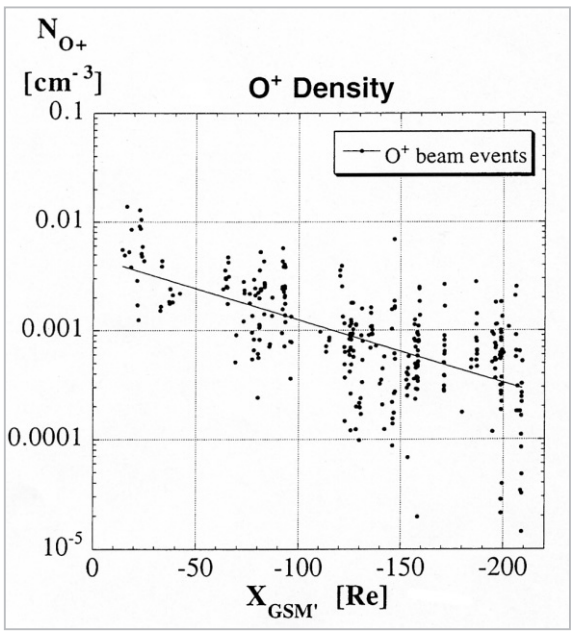

Fig.12 *Density distribution of oxygen ions in the magnetotail*

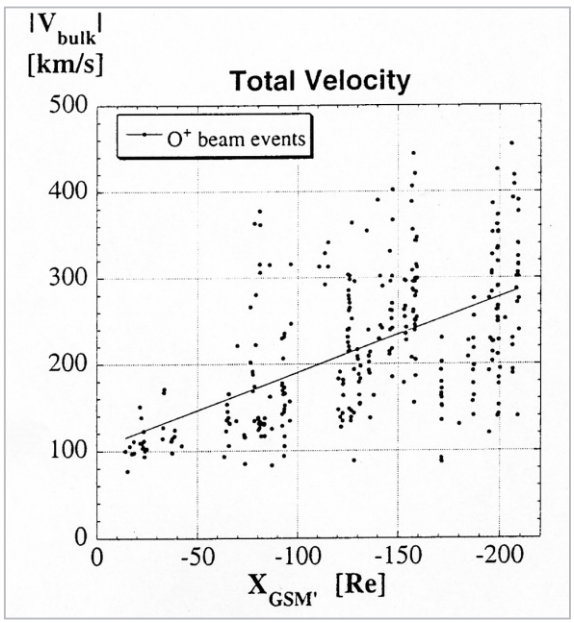

Fig.13 *Velocity distribution of oxygen ions in the magnetotail*

large, and velocity may even exceed 400 km/s in the tail.

The shape of the magnetosphere and the oxygen ion distribution were modeled to calculate the emission intensity. As shown in Fig.14, the magnetosphere is assumed to have an oval shape of X×Y = 30×20 R_E in the region beyond X =−50 R_E. In the region sunward of X =−50 R_E, the dayside magnetopause is set at X = 10 R_E, with a parabolic surface that connects smoothly with the magnetotail at X =−50 R_E. The GSM coordinates are used here (X axis: sunward; Z axis: points north in the plane containing the X axis and the geomagnetic axis).

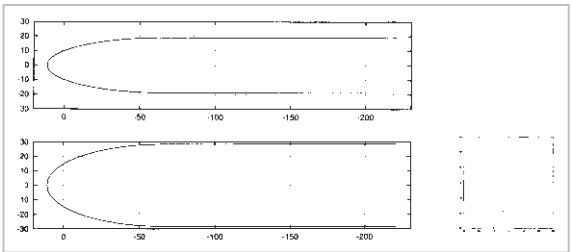

Fig.14 *The shape of the modeled magnetosphere*

Fig.15 shows the g-factors calculated using, as model values, the fitting lines of approximation for temperature, density, and bulk velocities of oxygen ions in the magnetosphere shown in Figs.11, 12, and 13. The horizontal and vertical axes represent the X-coordinate in the GSM system and the g-factor, respectively. Calculations were made by varying the oxygen ion bulk velocity parameter, for the model value V_b, for values $0.5V_b$ and $2V_b$, and for constant velocity of 200 km/s. When velocity is constant, the g-factor becomes a function only of temperature, remaining nearly constant regardless of X. However, if velocity is not constant, the g-factor changes significantly.

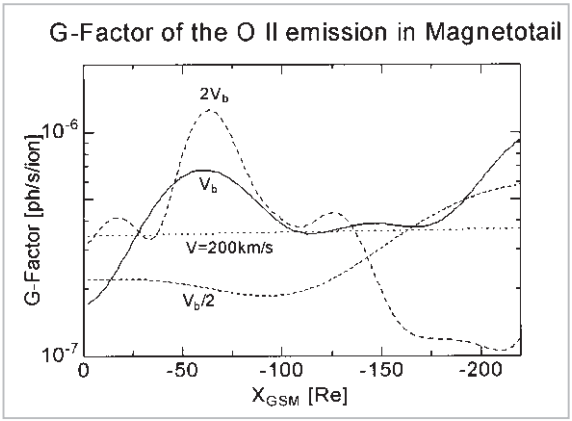

Fig.15 *The g-factors for oxygen ions in the magnetotail*

4.2 Intensity of Resonance-scattering emission from the Magnetotail

The distribution of O Ⅱ emission intensity in the magnetosphere was estimated using g-factors calculated in the previous section and the density distribution shown in Fig.12. However, since the spatial distribution of the oxygen ion beam has not been confirmed by observation, the temperature, density, and bulk velocity of oxygen ions were assumed to be a function only of X, being uniform in the Y and Z directions. The intensity of scattered emission in the magnetotail estimated here is the maximum expected value. Fig.16 shows the results of calculations, assuming a constant velocity of 200 km/s, regardless of X. In the two panels on the left, the Earth is located in the center on the left-hand side (X = 0, Y = 0). The upper left and lower left panels show the intensity of emission in the magnetotail as observed from within the equatorial plane (from the +Y direction) and from the north pole (from the +Z direction) of the magnetosphere, respectively. The right panel shows the distribution of the scattered emission intensity when the magnetotail is observed from the Earth (from the +X direction). Since the g-factor is nearly constant, the scattered emission intensity is proportional to the column density along the line-of-sight. The strongest

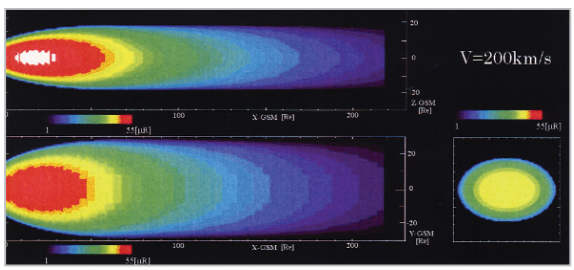

Fig.16 *Distribution of resonance-scattering emission intensity, assuming constant plasma velocity*

emission of 50 μR is seen in the region along the plasma sheet approximately 10-30 R_E from Earth. Even in the deepest region of the magnetotail located 200 R_E from Earth, intensity is still around 1 μR.

Fig.17 shows the results of calculations according to the bulk velocity model based on the Geotail satellite observation. The panels are arranged as in Fig.16. Since the g-factor in this model is a function of the distance from Earth, the maximum resonance-scattering emission intensity of 50 μR is seen near X = −50 R_E, where the product of the column density and g-factor is a maximum value. Minimum intensity is observed near X =−180 R_E in the plasma sheet. But even in this region, emission intensity exceeds 5 μR.

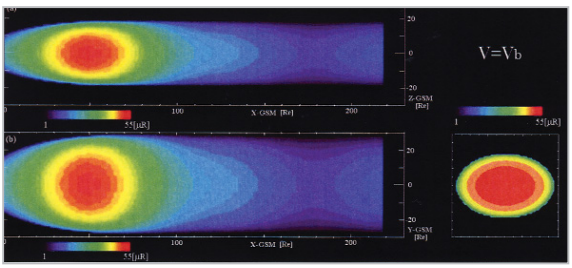

Fig.17 *Distribution of resonance-scattering emission intensity assuming bulk velocity, determined from results of Geotail satellite observation*

5 Observation Performance

Simple calculations in Sections 3 and 4 indicate that detection levels of 0.1 R for polar wind imaging and 5 μR for magnetotail imaging are sufficient for effective imaging observations. This section examines the feasibility of producing such an optical system. For the sake of simplicity, the measured count is assumed simply to be the sum of the signal and the noise of the detector. A value for noise is assumed based on calibration experiments performed on the ground. If both signal (*S*) and noise (*N*) are assumed to have normal distributions, the signal count must be greater than the statistical error of the measurement count (*S*+*N*), satisfying the conditional expression in Eq. (5.1), to distinguish the signal from noise (Fig.18). Here, the S/N ratio is defined as the ratio between and $\sqrt{S+N}$.

$$S > \sqrt{S+N} \qquad (5.1)$$

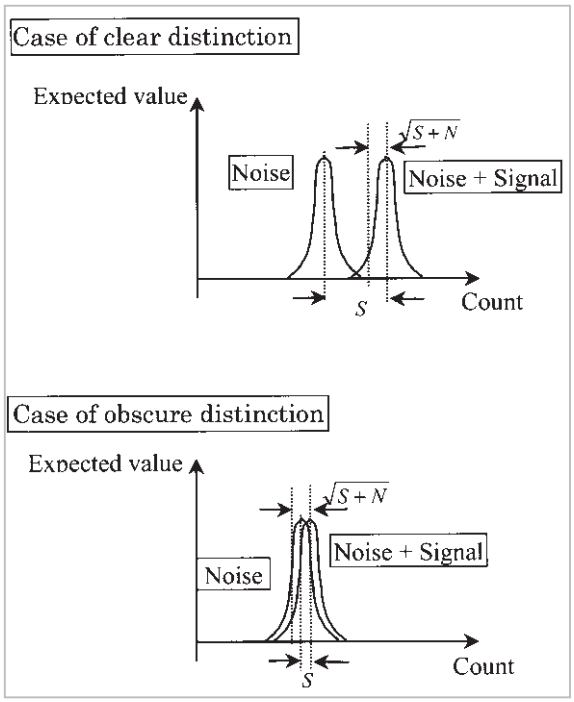

Fig.18 *Concept of separating signal from noise*

The intensities of signal (*S*) and noise (*N*) are expressed as follows:

$$S = I \cdot \pi\delta^2/4\pi \cdot \eta \cdot \pi a^2/4 \cdot T = 0.196 \cdot I \cdot \delta^2 \eta \cdot a^2 T \qquad (5.2)$$

$$N = \pi(aF\delta)^2 \cdot N_d \cdot T = \pi \cdot (F\delta)^2 \cdot N_d \cdot a^2 T \qquad (5.3)$$

Here, a is the telescope aperture, δ the angle of field-of-view (FOV), η the efficiency of the optical system, T the exposure time, I the intensity of the scattered emission, and N_d the detector noise count per unit area and time.

Fig.19 shows the S/N ratio as a function of scattered emission intensity (vertical axis) and exposure time (horizontal axis) under the following conditions. Micro Channel Plates (MCPs) are used as the detector; N_d is 0.5 /cm²/s. The efficiency of the optical system is 0.0004 for the instrument aboard the SS-520-2 rocket and 0.002 for the instrument with the new mirror. The angle of FOV, aperture, and F value are assumed to be 1°, 10 cm, and 1.0, respectively.

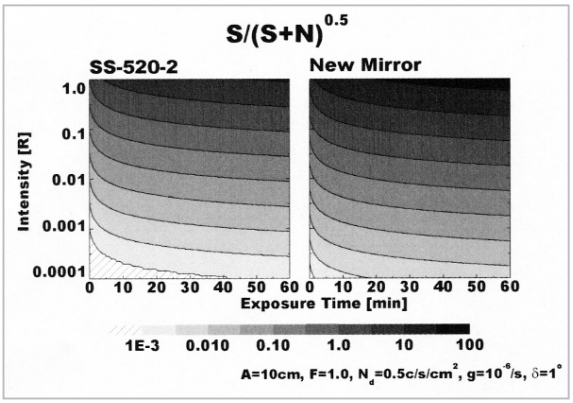

Fig.19 *S/N ratio shown as a function of scattered emission intensity and exposure time*

When the required observation condition is assumed to be an S/N ratio greater than 1, the instrument onboard the SS-520-2 rocket requires an exposure of approximately 1 hour to perform imaging observations of the polar wind given illumination levels of 0.1 R. In contrast, with the new mirror, imaging observations would require only 10 minutes. For magnetosphere imaging observations with maximum light intensity of 50 μR, an exposure of 1 hour using the new mirror would result in a S/N ratio of about 0.01. Since the S/N ratio is proportional to the telescope aperture and the square root of exposure, an aperture 30 times larger (or 500 cm) and an exposure 10 times longer (10 hours) would be required (for example) to achieve a S/N ratio of 1. However, such apertures are unrealistic, and the temporal resolution for such long exposures would be excessive relative to the response time of magnetospheric plasma variations. The resulting observations would have little significance. This has lead to heightened anticipation of the highly sensitive superconducting tunnel junction (STJ) device[38]. The features of the STJ detector are high quantum efficiency of 90%, generally noise-free counts, superior energy resolution, and capacity for cooling to 0.3 K. The STJ detector would achieve a 10-fold improvement in the sensitivity of the observation instrument. Since noise can be ignored, S/N ratio can be expected to improve by several orders of magnitude, enabling significant magnetosphere imaging observations with telescopes with apertures of several 10 cm, and at exposures of around 1 hour.

6 Conclusions

Both the polar wind and magnetotail have been found to be suitable as subjects of imaging observation replying on the resonance-scattering emission of oxygen ions contained therein. The optical system of the observation instrument must be capable of distinguishing light of 0.1 R and 5 μR from noise. Polar wind imaging has been demonstrated to be possible with a new coating for the mirror reflector. Magnetotail imaging observations, on the other hand, will require a new detector of STJ, in addition to the new coating. This represents a major line of inquiry for future research.

Imaging observations provide a global perspective on plasma distribution. This method will contribute to our understanding of the transport route and make it possible to distinguish between temporal and spatial variations. Information on the bulk velocity and temperature of oxygen ions may be obtained if satellites are deployed to make simultaneous *in-situ* measurements of plasma in the imaging region. This will enable more detailed discussions of density distribution. Additionally, the deployment of multiple imaging satellites for simultaneous observations from different angles will make it possible to perform real-time measurements of the 3-D density distribution of oxygen ions via tomography.

Numerous problems remain unresolved for near-Earth plasma, particularly the density and energy distributions of oxygen ions—such as the route and process of escape from the ionosphere, the mechanism of its supply to the magnetosphere, and the distribution of cold plasma in the plasma sheet. Remote-sensing methods have provided information on 2-D distributions of the plasma environment crucial for resolving such problems. They have also enabled us to view the unfolding of space environment disturbances such as geomagnet-

ic storms through variations in the general distribution of oxygen ions, thereby demonstrating the effectiveness of remote-sensing techniques as space weather monitoring systems. We expect these remote-sensing methods to make significant contributions to our understanding of planetary atmosphere and plasma escape and transport mechanisms.

References

1 Kaneda, E., M. Takagi, and N. Niwa, "Vacuum ultraviolet television camera", Proc. 12th Intnl. Symp. Space Tech. Sci., 233, Agne, Tokyo, 1977.

2 Frank, L. A., J. D. Craven, J. L. Burch, and J. D. Winningham, "Polar views of the earth's aurora with Dynamics Explorer", Geophys. Res. Lett., 9, 1,001, 1982.

3 Johnson, C. Y., J. M. Young, and J. C. Holmes, "Magnetoglow — A new geophysical resource", Science, 171, 379, 1971.

4 Chiu, Y. T., R. M. Robinson, G. R. Swenson, S. Chakrabarti, and D. S. Evans, "Imaging the outflow of ionospheric ions into the magnetosphere", Nature, 322, 441, 1986.

5 Meier, R. R., "Ultraviolet spectroscopy and remote sensing of the upper atmosphere", Space Sci. Rev., 58, 1, 1991.

6 Williams, D. J., E. C. Roelof, and D. G. Mitchell, "Global magnetospheric imaging", Rev. Geophys., 30, 183, 1992.

7 Meier, R. R., "The scattering rate of solar 834Å radiation by magnetospheric O^{+} and O^{++}", Geophys. Res. Lett., 17, 1,613, 1990.

8 Nakamura, M., I. Yoshikawa, A. Yamazaki, K. Shiomi, Y. Takizawa, M. Hirahara, K. Yamashita, Y. Saito, and W. Miyake, "Terrestrial plasmaspheric imaging by an extreme ultraviolet scanner on Planet-B", Geophys. Res. Lett., 27, 141, 2000.

9 Yoshikawa, I., A. Yamazaki, K. Shiomi, K. Yamashita, Y. Takizawa, and M. Nakamura, "Evolution of the outer plasmasphere during low geomagnetic activity observed by the EUV scanner onboard Planet-B", J. Geophys. Res., 105, 27,777, 2000.

10 Yoshikawa, I., A. Yamazaki, K. Shiomi, M. Nakamura, K. Yamashita, Y. Saito, M. Hirahara, Y. Takizawa, W. Miyake, and S. Matsuura, "Development of a compact EUV photometer for imaging the planetary magnetosphere", J. Geophys. Res., 106, 26,057, 2001.

11 Burch, J. L., S. B. Mende, D. G. Mitchell, T. E. Moore, C. J. Pollock, B. W. Reinisch, B. R. Sandel, S. A. Fuselier, D. L. Gallagher, J. L. Green, J. D .Perez, and P. H. Reiff, "Views of Earth's magnetosphere with the IMAGE satellite", Science, 291, 619, 2001.

12 Burch J. L., D. G. Mitchell, B. R. Sandel, P. C. Brandt, and M. Wüest, "Global dynamics of the plasmasphere and ring current during magnetic storms", Geophys. Res. Lett., 28, 1,159, 2001.

13 Sandel, B. R., R. A. King, W. T. Forrester, D. L. Gallagher, A. L. Broadfoot, and C. C. Curtis, "Initial results from the IMAGE extreme ultraviolet imager", Geophys. Res. Lett., 28, 1,439, 2001.

14 Axford, W. I., "The polar wind and the terrestrial helium budget", J. Geophys. Res., 73, 6,855, 1968.

15 Banks, P. M., and T. E. Holzer, "High-latitude plasma transport: The polar wind", J. Geophys. Res., 74, 6,317, 1969.

16 Chandler, M. O., J. H. Waite Jr., and T. E. Moore, "Observations of polar ion outflows", J. Geophys. Res., 96, 1,421, 1991.

17 Abe, T., B. A. Whalen, A. W. Yau, R. E. Horita, S. Watanabe, and E. Sagawa, "EXOS D (Akebono) suprathermal mass spectrometer observations of the polar wind", J. Geophys. Res., 98, 11,191, 1993.

18 Abe, T., S. Watanabe, B. A. Whalen, A. W. Yau, and E. Sagawa, "Observations of polar wind and thermal ion outflow by Akebono/SMS", J. Geomag. Geoelectr., 48, 319, 1996.

19 Yau, A. W., and M. Andre, "Sources of Ion Outflow in the High Latitude Ionosphere", Space Sci. Rev., 80, 1, 1997.

20 Mukai, T., M. Hirahara, S. Machida, Y. Saito, T. Terasawa, and A. Nishida, "Geotail observation of cold ion streams in the medium distance magnetotail lobe in the course of a substorm", Geophys. Res. Lett., 21, 1,023, 1994.

21 Hirahara, M., T. Mukai, T. Terasawa, S. Machida, Y. Saito, T. Yamamoto, and S. Kokubun, "Cold dense ion flows with multiple components observed in the distant tail lobe by Geotail", J. Geophys. Res., 101, 7,769, 1996.

22 Seki, K., M. Hirahara, T. Terasawa, I. Shinohara, T. Mukai, Y. Saito, S. Machida, and T. Yamamoto, "Coexistence of Earth-origin O^+ and solar wind-origin H^+/He^{++} in the distant magnetotail", Geophys. Res. Lett., 23, 985, 1996.

23 Seki, K., M. Hirahara, T. Terasawa, T. Mukai, and S. Kokubun, "Properties of He^+ beams observed by Geotail in the lobe/mantle regions: Comparison with O^+ beams", J. Geophys. Res., 104, 6,973, 1999.

24 Seki, K., R. C. Elphic, M. F. Thomsen, J. Bonnell, E. J. Lund, M. Hirahara, T. Terasawa, and T. Mukai, "Cold flowing O^+ beams in the lobe/mantle at Geotail: Does FAST observe the source?", J. Geophys. Res., 105, 15,931, 2000.

25 Seki, K., R. C. Elphic, M. Hirahara, T. Terasawa, and T. Mukai, "On atmospheric loss of oxygen ions from earth through magnetospheric processes", Science, 291, 1,939, 2001.

26 Yoshikawa, I., A. Yamazaki, K. Shiomi, K. Yamashita, Y. Takizawa, and M. Nakamura, "Photometric measurement of cold helium ions in the magnetotail by an EUV scanner onboard Planet-B: Evidence of the existence of cold plasmas in the near-Earth plasma sheet", Geophys. Res. Lett., 27, 3,567, 2000.

27 Tousey, R., "The extreme ultraviolet spectrum of the Sun", Space Sci. Rev., 2, 3, 1963.

28 Hinteregger, H. E., "Absolute intensity measurements in the extreme ultraviolet spectrum of solar radiation", Space Sci. Rev., 4, 461, 1965.

29 Rairden, R. L., L. A. Frank, and J. D. Craven, "Geocoronal imaging with Dynamics Explorer", J. Geophys. Res., 91, 13,613, 1986.

30 Palik, E D., ed. "Handbook of optical constants of solids", New York: Academic Press, 1985.

31 Palik, E. D., ed. "Handbook of optical constants of solids Ⅱ", Boston: Academic Press, 1991.

32 Yamazaki, A., S. Tashiro, Y. Nakasaka, I. Yoshikawa, W. Miyake, and M. Nakamura, "Sounding-rocket observation of O Ⅱ 83.4-nm emission over the polar ionosphere", Geophys. Res. Lett., 29, 2,005, doi:10.1029/2002gl014788, 2002.

33 Chakrabarti, S., J. Edelstein, R. A. M. Keski-Kuha, and F. T. Threat, "An 834Å reflective coating for magnetospheric imagery applications," Instru-mentation for Magnetospheric Imagery, Supriya Chakrabarti, Editor, Proc. SPIE, 1,744, 208, 1992.

34 Larruquert, J. I., and R. A. Keski-Kuha, "Multilayer coatings for narrowband imaging in the extreme ultraviolet", EUV, X-Ray, and Gamma-Ray Instrumentation for Astronomy Ⅷ, Oswald H. Siegmund, and Mark A. Gummin, Editors, Proc. SPIE, 3,114, 608, 1997.

35 Chappell, C. R., T. E. Moore, and J. H. Waite Jr., "The ionosphere as a fully adequate source of plasma for the earth's magnetosphere", J. Geophys. Res., 92, 5,896, 1987.

36 Orsini, S., M. Candidi, M. Stockholm, and H. Balsiger, "Injection of ionospheric ions into the plasma sheet", J. Geophys. Res., 95, 7,915, 1990.

37 Seki, K., Private communications.

38 Zehnder, A., C. W. Hagen, and W. Rothmund, "Superconducting tunneling junction detectors", EUV, X-ray, and Gamma-ray instrumentation for astronomy; H. S. Hudson., O. H. Siegmund, Editors, Proc. SPIE, 1,344, 286, 1990.

***YAMAZAKI Atsushi**, Ph. D.*

Research Fellow, Space Weather Group, Applied Research and Standards Division

Earth and Planetary Science

***MIYAKE Wataru**, Dr. Sci.*

Senior Researcher, Space Weather Group, Applied Research and Standards Division

Space Weather

***YOSHIKAWA Ichiro**, Ph. D.*

Associate Professor, Institute of Space and Astronautical Science

Earth and Planetary Science

***NAKAMURA Masato**, Ph. D.*

Professor, Institute of Space and Astronautical Science

Earth and Planetary Science

***TAKIZAWA Yoshiyuki**, Ph. D.*

Contract Researcher, Institute of Physical and Chemical Research